

RESEARCH ARTICLE | MARCH 17 2021

Temperature dependence of spin—orbit torque-driven magnetization switching in *in situ* grown Bi₂Te₃/MnTe heterostructures

Xiaoyang Liu; Di Wu; Liyang Liao; ... et. al



Appl. Phys. Lett. 118, 112406 (2021)

<https://doi.org/10.1063/5.0041062>



CrossMark

Articles You May Be Interested In

Interface dilution and morphology of CdTe/MnTe superlattices studied by small- and large-angle x-ray scattering

Journal of Applied Physics (May 2000)

Emergence of interfacial conduction and ferromagnetism in MnTe/InP

Appl. Phys. Lett. (November 2018)

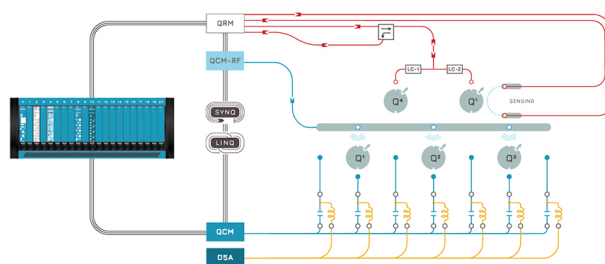
Thermoelectric study of crossroads material MnTe via sulfur doping

Journal of Applied Physics (March 2014)



Integrates all Instrumentation + Software for Control and Readout of

Superconducting Qubits
NV-Centers
Spin Qubits



Spin Qubits Setup

[find out more >](#)

Temperature dependence of spin–orbit torque-driven magnetization switching in *in situ* grown Bi₂Te₃/MnTe heterostructures

Cite as: Appl. Phys. Lett. **118**, 112406 (2021); doi: [10.1063/5.0041062](https://doi.org/10.1063/5.0041062)

Submitted: 18 December 2020 · Accepted: 3 March 2021 ·

Published Online: 17 March 2021







View Online



Export Citation



CrossMark

Xiaoyang Liu,^{1,2,3} Di Wu,⁴ Liyang Liao,⁵ Peng Chen,^{1,2,3} Yong Zhang,^{1,2,3}  Fenghua Xue,^{1,2,3}  Qi Yao,⁶ Cheng Song,⁵  Kang L. Wang,⁴  and Xufeng Kou^{1,6,a)} 

AFFILIATIONS

¹School of Information Science and Technology, ShanghaiTech University, Shanghai 201210, China

²Shanghai Institute of Microsystem and Information Technology, Chinese Academy of Sciences, Shanghai 200050, China

³University of Chinese Academy of Science, Beijing 101408, China

⁴Department of Electrical and Computer Engineering, University of California, Los Angeles, California 90095, USA

⁵Key Laboratory of Advanced Materials (MOE), School of Materials Science and Engineering, Tsinghua University, Beijing 100084, China

⁶ShanghaiTech Laboratory for Topological Physics, ShanghaiTech University, Shanghai 200031, China

^{a)} Author to whom correspondence should be addressed: kouxf@shanghaitech.edu.cn

ABSTRACT

We report the temperature dependence of the spin–orbit torque (SOT) in the *in situ* grown Bi₂Te₃/MnTe heterostructures by molecular beam epitaxy. By appropriately designing the film stack, robust ferromagnetic order with high Curie temperature and strong perpendicular magnetic anisotropy is established in the MnTe layer. Meanwhile, the sharp hetero-interface warrants highly efficient spin current injection from the conductive topological insulator (TI) channel. Accordingly, SOT-driven magnetization switching is observed up to 90 K with the critical current density within the 10⁶ A·cm⁻² range. More importantly, the temperature-dependent harmonic measurement data can be divided into two categories, namely, the spin Hall effect of the TI bulk states gives rise to a relatively small spin Hall angle in the high-temperature region, whereas the spin-momentum locking nature of the interfacial Dirac fermions leads to the enhancement of the SOT strength once the topological surface states become the dominant conduction channel at deep cryogenic temperatures. Our results offer direct evidence of the underlying mechanism that determines the SOT efficiency and may set up a suitable platform to realize TI-based spin–orbit applications toward room temperature.

Published under license by AIP Publishing. <https://doi.org/10.1063/5.0041062>

The use of spin–orbit coupling (SOC) to electrically manipulate the spin and magnetic orders has been considered as a promising route for realizing nonvolatile spintronics applications.^{1–3} In general, the spin Hall effect arisen from large SOC materials can exert spin–orbit torque (SOT) on the adjacent ferromagnetic (FM) layer with high efficiency.^{4–8} Compared with spin-transfer torque, this approach not only separates the spin current from the charge-based conduction path but also enables the magnetization switching with ultra-low current density.⁹ Accordingly, the emergence of spin-orbitronics has provided rich opportunities to engineer versatile spin–orbit effects by the electric field, and a variety of SOT-related phenomena have been demonstrated in magnetic heterostructures, which consist of different multi-functional materials.^{10–15}

In order to improve the charge-spin conversion efficiency, pursuing new materials with higher SOC strength is crucial. In this regard, topological insulators (TIs) with non-trivial band topology are expected to host spin–orbit coupling that is considerably stronger than conventional heavy-metal counterparts.¹⁶ Most importantly, the spin-momentum locking mechanism of the topological surface states (TSS) warrants highly spin-polarized surface current conduction, hence offering great potential for exploring SOTs.^{17,18} Following this scenario, magnetically doped TI (MTI) heterostructures [i.e., Cr-(BiSb)₂Te₃/(BiSb)₂Te₃] have been first synthesized and giant SOT-induced magnetization switching with ultra-low current density are demonstrated at cryogenic temperatures.^{19,20} Meanwhile, given the semiconductor

nature of the TI band structure, effective electric-field control of SOT is also realized in the MTI-based top-gate field-effect transistor device.²¹ To further overcome the low intrinsic Curie temperature (T_C) of MTI, recent advances have been made to integrate TIs with a suitable high- T_C magnetic layer so that the control of magnetization dynamics by SOT is achieved at room temperature.^{22–25} Based on these reported data, it is found that the SOT strength of the TI-based magnetic hybrid system is closely related to the hetero-interface conditions. For instance, the formation of defects and oxidation of the TI surface caused by the *ex situ* growth procedure (i.e., the as-grown TI sample will be exposed to air before loading into the magnetron sputtering chamber for the subsequent magnetic layer deposition) would inevitably degrade the interface quality and weaken the spin injection efficiency, while the *in situ* preparation of both the TIs and magnetic layers in one growth system has proven to be the better platform to produce giant SOT.^{26,27}

In this paper, we take full advantages of molecular beam epitaxy (MBE) to obtain the single-crystalline $\text{Bi}_2\text{Te}_3/\text{MnTe}$ heterostructures in which robust ferromagnetic order with strong perpendicular magnetic anisotropy (PMA) is maintained up to 130 K. Owing to the well-defined topological surface states at the sharp hetero-interface, pronounced spin current from the conductive TI channel is directly injected into the neighboring MnTe layer, hence yielding highly efficient SOT-driven magnetization switching above the liquid nitrogen temperature. Moreover, the extracted spin Hall angle of the TI/FM sample exhibits a distinctive temperature-dependent characteristic, which not only confirms the physical origin of the giant SOT but also quantifies different contributions from the dominant conduction channels during the switching process. Our results manifest the indispensable role of the topological surface states in SOT switching and may provide more insights into designing suitable TI-based magnetic film stacks for high-performance logic and memory devices.

Experimentally, the $\text{Bi}_2\text{Te}_3/\text{MnTe}$ heterostructures were grown on the semi-insulating GaAs(111)B substrate by MBE, as schematically illustrated in Fig. 1(a). With the adoption of an insulating CrSe buffer layer (4 unit-cell, 2.4 nm) and a moderate *in situ* post-annealing process, the single FM-phase MnTe layer with a thickness of 20 nm was obtained.²⁸ In the meantime, an 8 quintuple-layer (~ 8 nm) Bi_2Te_3 was chosen as the top layer because of its similar resistivity to the underneath MnTe channel, and such matched impedance ensures sufficient anomalous Hall signals from the MnTe layer while preventing the hazardous current shunting effect during the SOT switching measurements. From both the angle- [Fig. 1(b)] and temperature-dependent [Fig. 1(c)] magneto-transport data, it is seen that the marked anomalous Hall effect (AHE) with nearly square-shape hysteresis R_{xy} loops is observed up to 130 K when the applied magnetic field B_z is perpendicular to the film. In contrast, a large in-plane magnetic field of $|B_x| > 6$ T is required to saturate the magnetization, which again verifies the strong PMA property of the as-grown sample. Along with the field-cooling magnetization curve that follows the classic Curie-Weiss law [Fig. 1(d)],²⁹ it is concluded that the high- T_C magnetic order formed in our high-quality $\text{Bi}_2\text{Te}_3/\text{MnTe}$ heterostructures may facilitate the investigations of spin-orbit physics at higher temperatures as compared with the MTI/TI counterparts.

Accordingly, Fig. 2 presents the SOT-driven magnetization switching results of the $\text{Bi}_2\text{Te}_3/\text{MnTe}$ sample up to 90 K. The epitaxial film was first fabricated into the six-probe Hall-bar device with the channel geometry of $20 \mu\text{m}$ (width) $\times 90 \mu\text{m}$ (length) using standard

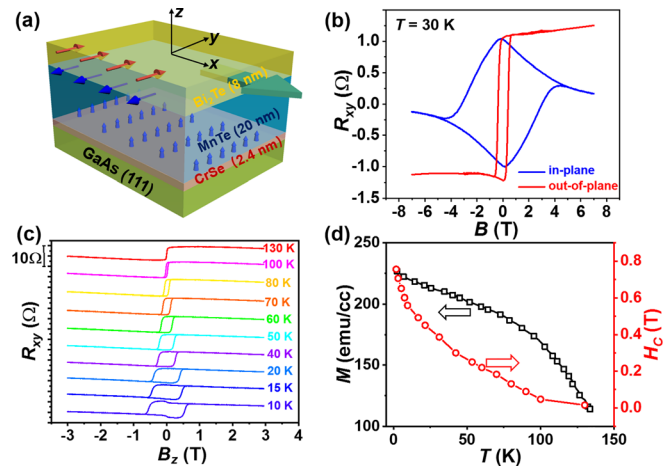


FIG. 1. (a) Schematic of the *in situ* MBE-grown $\text{Bi}_2\text{Te}_3(8 \text{ nm})/\text{MnTe}(20 \text{ nm})$ heterostructures. A 4 unit-cell ($\sim 2.4 \text{ nm}$) insulating CrSe is incorporated as the buffer layer for the subsequent FM-phase MnTe epitaxial growth. The red and blue arrows in the top TI layer represent the electron spin directions. (b) Typical anomalous Hall resistance R_{xy} of the sample measured at $T = 30 \text{ K}$ as functions of both the in-plane (blue) and out-of-plane (red) magnetic fields. (c) Temperature-dependent R_{xy} results showing robust ferromagnetic order up to 130 K. (d) Temperature-dependent magnetic moment (black squares) and coercivity field (red circles). An external perpendicular magnetic field of 20 mT is used during the field-cooling measurement.

photolithography and ion-beam etching process, as displayed in Fig. 2(a). After device fabrication, DC-dependent magneto-transport experiments were carried out with the presence of a constant magnetic field along the current direction (i.e., to break the inversion-symmetry of the system so that the deterministic switching is allowed¹⁹). By varying the applied write current amplitude (i.e., with the fixed pulse width of 1 ms and read current of $20 \mu\text{A}$), the sign of the anomalous Hall resistance signal (i.e., magnetization direction) is modulated, and its corresponding current-induced switching polarity can be elaborated on the basis of the SOT mechanism. Specifically, given the bilayer structure shown in Fig. 1(a), when the charge current (I_{DC}) is applied along the $+x$ -axis, the spin current accumulated at the $\text{Bi}_2\text{Te}_3/\text{MnTe}$ interface (i.e., bottom surface of the TI layer) is expected to host the spin-polarization toward the $-y$ -direction, which in turn produces the effective spin-orbit field ($\mathbf{B}_{\text{SO}} = I_{\text{DC}} \lambda_{\text{SO}} \boldsymbol{\sigma} \times \mathbf{M}$, where λ_{SO} is the characteristic coefficient gauging the SOT strength and $\boldsymbol{\sigma}$ is the electron spin) to manipulate the magnetic moment (\mathbf{M}) of the MnTe layer. Under such circumstances, the resulting spin-orbit torque $\boldsymbol{\tau}_{\text{SO}} = -\gamma \mathbf{M} \times \mathbf{B}_{\text{SO}} \propto \mathbf{M} \times (\mathbf{M} \times \boldsymbol{\sigma})$ (where γ is the gyromagnetic ratio) will stabilize the magnetization along the $+z$ -direction when the in-plane magnetic field B_x is applied parallel to I_{DC} [upper panel of Fig. 2(b)], whereas the reversal of the DC bias would switch the initial $+M_z$ state to the opposite direction [lower panel of Fig. 2(b)]. Consequently, as the DC level is successively reduced from $+8 \text{ mA}$ in the presence of $B_x = +40 \text{ mT}$, the measured $R_{xy} = +1 \Omega$ remains constant until the positive-to-negative transition occurs at $I_{\text{DC}} < -4 \text{ mA}$ (i.e., equivalent to a critical current density of $6.6 \times 10^6 \text{ A cm}^{-2}$). On the contrary, clockwise hysteretic behavior of the $R_{xy}-I_{\text{DC}}$ loop is observed for the $B_x = -40 \text{ mT}$ case with the same critical switching current of $\pm 4 \text{ mA}$, and the B_x -fixed, I_{DC} -dependent transport data all retain the nearly 100% switching feature with similar chiral contours

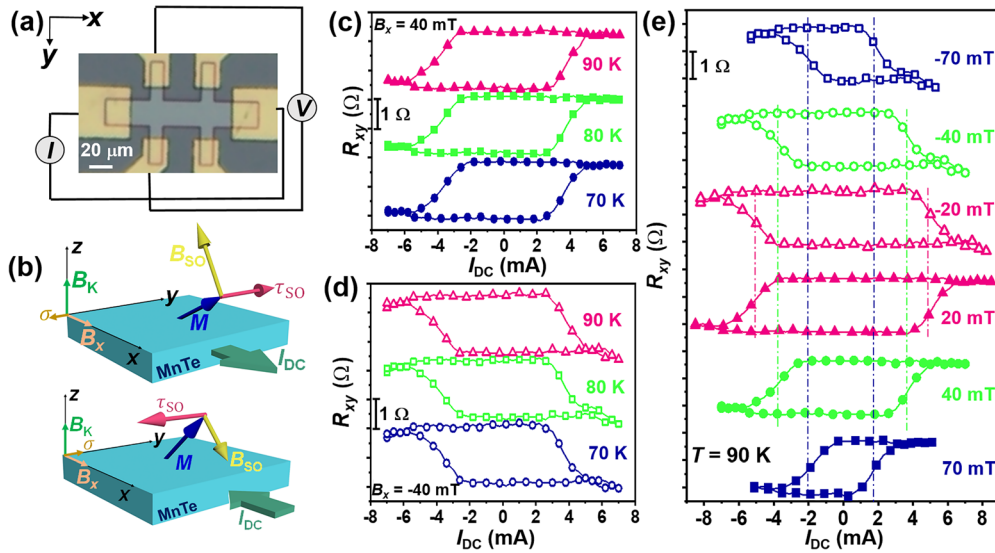


FIG. 2. (a) Optical microscopy image of the fabricated six-probe Hall-bar device with the channel geometry of 20 μm (width) \times 90 μm (length). (b) Illustrations of the effective spin-orbit field (B_{SO}) and damping-like torque (τ_{SO}) with respect to the applied DC (I_{DC}) and the assisted in-plane magnetic field (B_x) directions. B_K is the anisotropy field of the MnTe layer and σ is the electron spin polarization of the bottom TI surface states at the hetero-interface. (c) and (d) SOT-driven magnetization switching in the $\text{Bi}_2\text{Te}_3/\text{MnTe}$ heterostructures at $T=70$ K, 80, and 90 K. The applied in-plane magnetic field B_x is chosen as (c) +40 mT and (d) -40 mT, respectively. (e) Current-induced switching hysteresis loops under different in-plane magnetic fields at $T=90$ K.

from 70 K to 90 K, as confirmed in Figs. 2(c) and 2(d). Furthermore, the magnetization switching hysteresis loops under different external in-plane magnetic fields are depicted in Fig. 2(e). In addition to the initial configuration between I_{DC} and B_x that governs the SOT phase diagram, it is clear that the critical switching current discloses a negative correlation with the assisted in-plane magnetic field. As illustrated in Fig. 2(b), a larger B_x -field helps to tilt the magnetic moment close to the x-axis, hence increasing the perpendicular component of the effective SOT field given that B_{SO} is strictly orthogonal to M . As a result, a lower DC can meet the deterministic switching requirement, namely, the amplitude of B_{SO} along the z-axis needs to be larger than the out-of-plane anisotropy field B_K of the MnTe layer, and our results are consistent with those reported in the TI-based magnetic heterostructures.^{19,20}

To quantify the SOT strength of the $\text{Bi}_2\text{Te}_3/\text{MnTe}$ system, we further probed the SOT-tailored magnetic precession via second harmonic measurements at different temperatures. Generally, when a sinusoidal input current passes through the TI channel, the generated AC effective spin-orbit field would cause the magnetization of MnTe to precess around its equilibrium position with identical oscillating frequency.^{30,31} Thanks to the negligible planar Hall effect of our $\text{Bi}_2\text{Te}_3/\text{MnTe}$ sample (i.e., 0.02 Ω vs $R_{xy} = 1 \Omega$), the magnitude of B_{SO} can be determined by recording both the 1st (R_{xy}^{ω}) and 2nd ($R_{xy}^{2\omega}$) harmonic components of the anomalous Hall resistance,^{32,33}

$$R_{xy}^{2\omega} = \frac{R_{xy}^{\omega}}{2} \cdot \frac{B_{\text{SO}}}{|B_x| - B_K} + R_{\text{thermal}} \frac{B_x}{|B_x|}, \quad (1)$$

where R_{thermal} stands for the 2nd harmonic response from the anomalous Nernst and/or spin Seebeck effects. Subsequently, Figs. 3(a) and 3(b) exemplify one set of the experimental results measured at

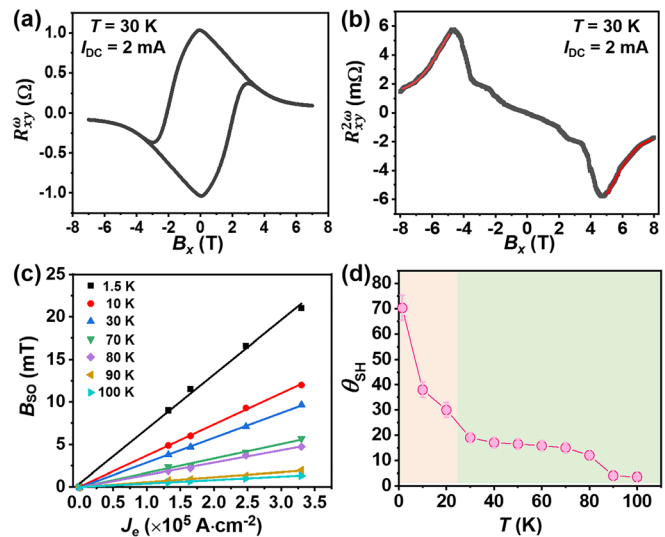


FIG. 3. (a) First and (b) second harmonic anomalous Hall resistances as a function of the in-plane magnetic field at $T=30$ K and $I_{\text{DC}}=2$ mA. In order to exclude the 2nd harmonic response from thermoelectric effects, only the $[\pm 5 \text{ T}, \pm 8 \text{ T}]$ high-field data are used to estimate the effective SOT field. (c) Temperature-dependent effective spin-orbit field B_{SO} extracted from Eq. (1). The linear relationship between B_{SO} and charge current density J_e confirms the absence of Joule heating and other non-linear effects during the measurement. (d) Temperature dependence of the spin Hall angle in $\text{Bi}_2\text{Te}_3/\text{MnTe}$ heterostructures. The source of the error bar here mainly comes from the fitting error during the data processing procedure.

$T = 30$ K with a fixed lock-in frequency of 15.2 Hz and $I_{DC} = 2$ mA. According to Eq. (1), when the applied magnetic field is high enough (i.e., $B_x \gg B_K$), the magnetization of the MnTe layer becomes in-plane, hence leaving the thermoelectric effect contribution constant. Consequently, by fitting the high-field $R_{xy}^{2\omega} - B_x$ curve (i.e., the red lines in the $[\pm 5$ T, ± 8 T] regime), the intrinsic strength of B_{SO} can be calculated. Figure 3(c) summarizes the effective SOT field as a function of the applied charge current density (J_e) where the linear relationship is identified from 1.5 K to 100 K, again indicating the absence of Joule heating and other non-linear effects in the examined current range.³⁴ By further converting the slope of the $B_{SO}-J_e$ into the spin Hall angle $\theta_{SH} = (B_{SO}/J_e) \cdot (2eM_s t_{MnTe}/\hbar)$ [i.e., where e is the electron charge, t_{MnTe} is the MnTe layer thickness, M_s is the saturated magnetic moment shown in Fig. 1(d), and \hbar is the reduced Planck constant], we plot its temperature-dependent result in Fig. 3(d). Strikingly, as the sample is cooled down below T_C , θ_{SH} first increases slowly from 10 to 15 in the high-temperature region (25 K $< T < 80$ K), and it then experiences a dramatic enhancement up to 78 at $T = 1.5$ K. (i.e., as a comparison, the values of θ_{SH} in heavy-metal systems always exhibit a single scaling law with temperature owing to its bulk SOC property^{34,35}). In addition, we need to point out that the SOT measured in this work is the damping-like torque since B_x is along the same direction of I_{DC} . In fact, we have also calibrated the transverse-field-like torque by tilting the initial magnetization within the yz -plane with the assisted magnetic field B_y , yet the corresponding second harmonic signals are too small to be detected.

In order to understand this unique temperature dependence of the SOT efficiency in the Bi_2Te_3 /MnTe heterostructures, we first recall that the spin Hall angle is associated with both M_s and B_{SO}/J_e once the multilayer structure is given. From the field-cooling data in Fig. 1(d), it is revealed that the magnetization of the sample gradually becomes saturated as the base temperature approaches 1.5 K. Therefore, the M_s variation itself cannot explain the sharp increase in θ_{SH} when $T < 25$ K. Alternatively, it is known that when the bulk conduction is suppressed at deep cryogenic temperatures, majority electrons would transport along the topological surface states. Under this condition, these surface Dirac fermions are tightly spin-polarized with respect to their momentum direction; in other words, the TI surface states act as a source of spin regeneration, which ensures a non-vanishing spin density of the charge current as well as guarantees the highly efficient interfacial spin injection with giant $\theta_{SH} \gg 1$.⁹ On the other hand, the increased thermal activation at elevated temperatures may drive the dominant conduction channel from TSS to the bulk. Instead of the spin-momentum locking mechanism, the SOT strength of the TI bulk states, which stems from the spin Hall effect, is expected to suffer from various spin diffusion/scattering processes (i.e., similar to the heavy-metal cases), thereafter resulting in the reduction of θ_{SH} in the high-temperature region. To validate the above argument, we have grown an additional 8 QL Bi_2Te_3 thin film with identical growth recipe and traced the relevant temperature-dependent magneto-resistance (MR) data. As highlighted in Fig. 4(a), the pronounced weak anti-localization effect with linear MR cusp in the low-field region (i.e., which serves as the hallmark of TSS conduction^{36,37}) happens to appear when $T < 30$ K. Likewise, the temperature-dependent conductivity curve [red circles of Fig. 4(b)] also displays a saturation trend as the Bi_2Te_3 sample is cooled down to deep cryogenic temperatures, thus implying the suppression of the thermal-activated bulk conduction.

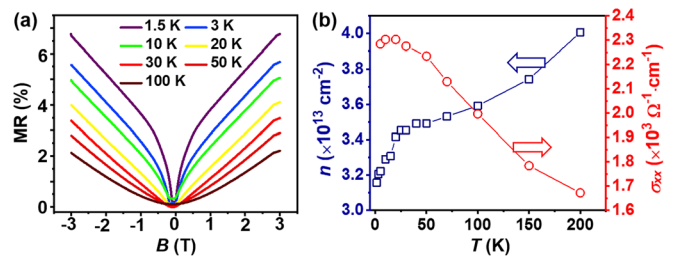


FIG. 4. (a) Temperature-dependent magneto-resistance (MR) results of the pure 8 nm Bi_2Te_3 thin film from 1.5 K to 100 K. The onset of the weak anti-localization effect manifests the dominant conduction channel of the topological surface states below 25 K. (b) Temperature dependences of carrier concentration n (blue squares) and electrical conductivity σ_{xx} (red circles) of the Bi_2Te_3 sample. The saturation of the $\sigma_{xx} - T$ slope suggests the bulk-to-TSS transition at low temperatures.

Because of the consistency between the such onset temperature and the turning point of the $\theta_{SH}(T)$ slope [Fig. 3(d)], we may conclude that the enhancement of the spin Hall angle is related to the bulk-to-TSS transition of the TI layer. Here, it is worth noting that similar temperature-dependent SOT behaviors have also been discovered in other TI-based magnetic heterostructures [e.g., $Bi_2Se_3/CoFeB$ and $Cr-(BiSb)_2Te_3/(BiSb)_2Te_3$] recently, again unveiling the universal interplay between the TSS/bulk contributions and the SOT efficiency of TIs.^{38,39}

In conclusion, endowed by both the high- T_C magnetic order and atomically sharp interface in the *in situ* MBE-grown Bi_2Te_3 /MnTe heterostructures, we have demonstrated the SOT-driven magnetization switching up to 90 K with low critical current density comparable to previous reports. In addition, the temperature-dependent spin Hall angle diagram has emphasized the importance of the topological surface states on the SOT strength. In order to maintain the giant spin-orbit efficiency at high temperatures, future work can be designed to improve the spin-polarized current contribution through appropriate structural engineering (e.g., the adoption of modulation-doping strategy to reduce bulk conduction and the use of the Rashba effect to align electron spins at the hetero-interface). Likewise, the introduction of the top-gate device structure may help the electric-field control of the SOT strength by effective Fermi level tuning and facilitate the TI-based spintronics applications toward room temperature.

This work was supported by the National Key R&D Program of China (Contract No. 2017YFA0305400); the National Natural Science Foundation of China (Grant No. 61874172); the Strategic Priority Research Program of Chinese Academy of Sciences (Grant No. XDA18010000); the Major Project of Shanghai Municipal Science and Technology (Grant No. 2018SHZDZX02); and the ShanghaiTech Quantum Device and Soft Matter Nano-fabrication Labs (SMN180827). X.K. acknowledges the support from the Merck POC Program.

DATA AVAILABILITY

The data that support the findings of this study are available from the corresponding author upon reasonable request.

REFERENCES

1. J. Sinova, S. O. Valenzuela, J. Wunderlich, C. H. Back, and T. Jungwirth, *Rev. Mod. Phys.* **87**(4), 1213 (2015).

- ²S. Bhatti, R. Sbiaa, A. Hirohata, H. Ohno, S. Fukami, and S. N. Piramanayagam, *Mater. Today* **20**(9), 530 (2017).
- ³A. Manchon, J. Železný, I. M. Miron, T. Jungwirth, J. Sinova, A. Thiaville, K. Garello, and P. Gambardella, *Rev. Mod. Phys.* **91**(3), 035004 (2019).
- ⁴A. Manchon and S. Zhang, *Phys. Rev. B* **79**(14), 094422 (2009).
- ⁵I. M. Miron, G. Gaudin, S. Auffret, B. Rodmacq, A. Schuhl, S. Pizzini, J. Vogel, and P. Gambardella, *Nat. Mater.* **9**(3), 230 (2010).
- ⁶L. Liu, T. Moriyama, D. C. Ralph, and R. A. Buhrman, *Phys. Rev. Lett.* **106**(3), 036601 (2011).
- ⁷L. Q. Liu, C. F. Pai, Y. Li, H. W. Tseng, D. C. Ralph, and R. A. Buhrman, *Science* **336**(6081), 555 (2012).
- ⁸L. Q. Liu, O. J. Lee, T. J. Gudmundsen, D. C. Ralph, and R. A. Buhrman, *Phys. Rev. Lett.* **109**(9), 096602 (2012).
- ⁹K. L. Wang, X. F. Kou, P. Upadhyaya, Y. B. Fan, Q. M. Shao, G. Q. Yu, and P. K. Amiri, *Proc. IEEE* **104**(10), 1974 (2016).
- ¹⁰K. S. Ryu, L. Thomas, S. H. Yang, and S. Parkin, *Nat. Nanotechnol.* **8**(7), 527 (2013).
- ¹¹J. C. Rojas Sanchez, L. Vila, G. Desfonds, S. Gambarelli, J. P. Attane, J. M. De Teresa, C. Magen, and A. Fert, *Nat. Commun.* **4**, 2944 (2013).
- ¹²H. Kurebayashi, J. Sinova, D. Fang, A. C. Irvine, T. D. Skinner, J. Wunderlich, V. Novak, R. P. Campion, B. L. Gallagher, E. K. Vehstedt, L. P. Zarbo, K. Vyborny, A. J. Ferguson, and T. Jungwirth, *Nat. Nanotechnol.* **9**(3), 211 (2014).
- ¹³G. Q. Yu, P. Upadhyaya, Y. B. Fan, J. G. Alzate, W. J. Jiang, K. L. Wong, S. Takei, S. A. Bender, L. T. Chang, Y. Jiang, M. R. Lang, J. S. Tang, Y. Wang, Y. Tserkovnyak, P. K. Amiri, and K. L. Wang, *Nat. Nanotechnol.* **9**(7), 548 (2014).
- ¹⁴S. Fukami, T. Anekawa, C. Zhang, and H. Ohno, *Nat. Nanotechnol.* **11**(7), 621 (2016).
- ¹⁵C. O. Avci, A. Quindeau, C. F. Pai, M. Mann, L. L. Caretta, A. S. Tang, M. C. Onbasli, C. A. Ross, and G. S. Beach, *Nat. Mater.* **16**(3), 309 (2017).
- ¹⁶D. Pesin and A. H. MacDonald, *Nat. Mater.* **11**(5), 409 (2012).
- ¹⁷A. R. Mellnik, J. S. Lee, A. Richardella, J. L. Grab, P. J. Mintun, M. H. Fischer, A. Vaezi, A. Manchon, E. A. Kim, N. Samarth, and D. C. Ralph, *Nature* **511**(7510), 449 (2014).
- ¹⁸Y. Tokura, K. Yasuda, and A. Tsukazaki, *Nat. Rev. Phys.* **1**(2), 126 (2019).
- ¹⁹Y. B. Fan, P. Upadhyaya, X. F. Kou, M. R. Lang, S. Takei, Z. X. Wang, J. S. Tang, L. He, L. T. Chang, M. Montazeri, G. Q. Yu, W. J. Jiang, T. X. Nie, R. N. Schwartz, Y. Tserkovnyak, and K. L. Wang, *Nat. Mater.* **13**(7), 699 (2014).
- ²⁰K. Yasuda, A. Tsukazaki, R. Yoshimi, K. Kondou, K. S. Takahashi, Y. Otani, M. Kawasaki, and Y. Tokura, *Phys. Rev. Lett.* **119**(13), 137204 (2017).
- ²¹Y. B. Fan, X. F. Kou, P. Upadhyaya, Q. M. Shao, L. Pan, M. R. Lang, X. Y. Che, J. S. Tang, M. Montazeri, K. Murata, L. T. Chang, M. Akyol, G. Q. Yu, T. X. Nie, K. L. Wong, J. Liu, Y. Wang, Y. Tserkovnyak, and K. L. Wang, *Nat. Nanotechnol.* **11**(4), 352 (2016).
- ²²J. Han, A. Richardella, S. A. Siddiqui, J. Finley, N. Samarth, and L. Liu, *Phys. Rev. Lett.* **119**(7), 077702 (2017).
- ²³Y. Wang, D. Zhu, Y. Wu, Y. Yang, J. Yu, R. Ramaswamy, R. Mishra, S. Shi, M. Elyasi, K. L. Teo, Y. Wu, and H. Yang, *Nat. Commun.* **8**(1), 1364 (2017).
- ²⁴Q. M. Shao, H. Wu, Q. J. Pan, P. Zhang, L. Pan, K. Wong, X. Y. Che, and K. L. Wang, in International Electron Devices Meeting (IEDM) (2018), p. 36.3.1.
- ²⁵H. Wu, P. Zhang, P. Deng, Q. Q. Lan, Q. J. Pan, S. A. Razavi, X. Y. Che, L. Huang, B. Q. Dai, K. Wong, X. F. Han, and K. L. Wang, *Phys. Rev. Lett.* **123**(20), 207205 (2019).
- ²⁶N. H. D. Khang, Y. Ueda, and P. N. Hai, *Nat. Mater.* **17**(9), 808 (2018).
- ²⁷M. Dc, R. Grassi, J. Y. Chen, M. Jamali, D. Reifsnnyder Hickey, D. Zhang, Z. Zhao, H. Li, P. Quarterman, Y. Lv, M. Li, A. Manchon, K. A. Mkhoyan, T. Low, and J. P. Wang, *Nat. Mater.* **17**(9), 800 (2018).
- ²⁸P. Chen, Y. Zhang, Q. Yao, F. G. Tian, L. Li, Z. K. Qi, X. Y. Liu, L. Y. Liao, C. Song, J. Y. Wang, J. Xia, G. Li, D. M. Burn, G. van der Laan, T. Hesjedal, S. L. Zhang, and X. F. Kou, *Nano Lett.* **20**(3), 1731 (2020).
- ²⁹J. M. Coey, *Magnetism and Magnetic Materials* (Cambridge University Press, 2010).
- ³⁰K. Garello, I. M. Miron, C. O. Avci, F. Freimuth, Y. Mokrousov, S. Blugel, S. Auffret, O. Boule, G. Gaudin, and P. Gambardella, *Nat. Nanotechnol.* **8**(8), 587 (2013).
- ³¹J. Kim, J. Sinha, M. Hayashi, M. Yamanouchi, S. Fukami, T. Suzuki, S. Mitani, and H. Ohno, *Nat. Mater.* **12**(3), 240 (2013).
- ³²C. O. Avci, K. Garello, C. Nistor, S. Godey, B. Ballesteros, A. Mugarza, A. Barla, M. Valvidares, E. Pellegrin, A. Ghosh, I. M. Miron, O. Boule, S. Auffret, G. Gaudin, and P. Gambardella, *Phys. Rev. B* **89**(21), 214419 (2014).
- ³³H. Wu, Y. Xu, P. Deng, Q. J. Pan, S. A. Razavi, K. Wong, L. Huang, B. Q. Dai, Q. M. Shao, G. Q. Yu, X. F. Han, J. C. Rojas-Sanchez, S. Mangin, and K. L. Wang, *Adv. Mater.* **31**(35), 1901681 (2019).
- ³⁴W. Seung Ham, S. H. Kim, D. H. Kim, K. J. Kim, T. Okuno, H. Yoshikawa, A. Tsukamoto, T. Moriyama, and T. Ono, *Appl. Phys. Lett.* **110**(24), 242405 (2017).
- ³⁵W. Skowronski, M. Cecot, J. Kanak, S. Ziętek, T. Stobiecki, L. Yao, S. van Dijken, T. Nozaki, K. Yakushiji, and S. Yuasa, *Appl. Phys. Lett.* **109**(6), 062407 (2016).
- ³⁶H. Z. Lu, J. R. Shi, and S. Q. Shen, *Phys. Rev. Lett.* **107**(7), 076801 (2011).
- ³⁷A. Roy, S. Guchhait, S. Sonde, R. Dey, T. Pramanik, A. Rai, H. C. P. Movva, L. Colombo, and S. K. Banerjee, *Appl. Phys. Lett.* **102**(16), 163118 (2013).
- ³⁸Y. Wang, P. Deorani, K. Banerjee, N. Koirala, M. Brahlek, S. Oh, and H. Yang, *Phys. Rev. Lett.* **114**(25), 257202 (2015).
- ³⁹X. Y. Che, Q. J. Pan, B. Vareskic, J. Zou, L. Pan, P. Zhang, G. Yin, H. Wu, Q. M. Shao, P. Deng, and K. L. Wang, *Adv. Mater.* **32**(16), e1907661 (2020).